Simulations of a LDPE Reactor Using Computational Fluid Dynamics

Nolan K. Read, Simon X. Zhang, and W. Harmon Ray
Dept. of Chemical Engineering, University of Wisconsin–Madison, Madison, WI 53706

Computational fluid dynamics methods are used to provide three-dimensional simulations of a low-density polyethylene (LDPE) autoclave reactor under normal operating conditions. For the conditions used, the reactor is not very well mixed; thus, the common model approximation of a perfectly stirred reactor is not warranted. The simulations verify the sensitive nature of the polymerization reactors and indicate a need for optimizing operating parameters.

Introduction

Low-density polyethylene (LDPE) a commodity polymer used in a wide variety of applications such as plastic bags and wrappings, cable insulation, and coatings, can be produced by either tubular or autoclave processes. Both processes involve free-radical polymerization of ethylene at high temperature and high pressure. The tubular process employs a long tubular reactor that enhances heat removal. The autoclave process involves an adiabatic autoclave reactor. As of 1992, LDPE accounted for 40% of total polyethylene production globally. Each process produced roughly 50% of the preceding figure. This article will concentrate on the autoclave operation.

Characteristics of the autoclave operation include short residence times and short initiator half-lives so that mixing times are comparable to reaction times. Because of this imperfect mixing, some areas of the reactor can produce polymers with different physical properties as compared with those produced in other zones. This arises because in the mixing zones there are different polymerization reaction rates and different concentration and temperature gradients. Thermal runaways or "decomps," which cause a buildup of pressure and temperature in the reactor and often cause the explosive discharge of ethylene and (by-)products into the environment, are known to occur in this reactor; once initiated the runaway can be completed in a few seconds (Huffman et al., 1974; Sullivan and Shannon, 1992; Zhang et al., 1996). It is believed (Gardner, 1975) that this phenomenon may be caused by local hot spots in the reactor. These hot spots can be caused by imperfect mixing.

Because of the imperfect mixing in these autoclave reactors, compartmental models, which "divide" the reactors into different parts corresponding to the mixing in that part, are widely employed (Marini and Georgakis, 1984a,b; Ochs et al., 1996). The idea is that the whole reactor can be modeled as a combination of "ideal" reactors with exchange of mass and energy between each of the ideal reactors. However, some basic understanding of the mixing phenomena in autoclave reactors is necessary to build good compartmental models.

This research attempts to obtain a better understanding of the coupled mixing and reaction in the autoclave reactor by solving a three-dimensional model of the reactor using the Computational Fluid Dynamics (CFD) package (Fluent Inc., 1993). This representation includes the reactor, rotating impeller, polymerization kinetics, k-ϵ turbulence model, and a turbulent reaction-rate model. Since there is no symmetry to simplify the problem, a full 3-D simulation is undertaken; thus, these simulations are very computationally intensive.

Four cases are studied: the first with one "slow" initiator, and the others with mixed initiators—one a fast decomposing initiator, the other slower. Of primary interest in these cases are the flow lines, concentration gradients, and temperature gradients for these different operating conditions. A good understanding of these phenomena will lead to better kinetic and compartmental models for LDPE polymerization. In addition, because imperfect mixing is long suspected to be responsible for irregular decomposition in LDPE autoclave, a good model of this process is important for both economic reasons and safety issues.

Literature Survey

Mixing can be of two types, macromixing and micromixing. Phenomena such as channeling and dead zones in a reactor are a sign of imperfect macromixing. In other words,

Correspondence concerning this article should be addressed to W. H. Ray.
Present addresses of: N. K. Read, DuPont CRD, Parkersburg, NY; S. X. Zhang, Exxon Polymers, Baytown, TX.

macromixing is concerned with how well the bulk fluid heterogeneities are reduced; residence time distribution via, for instance, tracer studies is a good indicator of degree of macromixing. In contrast, micromixing is concerned with mixing on the molecular scale. Molecular diffusion would be an example of micromixing.

Sometimes it is not an easy task to delineate macro- and micromixing models since if one assumes a model (e.g., a continuously stirred tank reactor or CSTR), one has specified both macro- and micromixing in the reactor. According to Smit (1992), any model that explains the "slowness" of mixing will be able to describe experimentally determined variables such as initiator consumption. Smit (1992) prefers physically realistic models to describe micromixing. Therefore, in this discussion, the following categories are used: compartmental models are classified as macromodels, and any phenomenological models that try to describe the decay or increase of segregation (e.g., diffusion effects) are classified as micromodels.

Macromixing in LDPE reactors

Generally, popular models of macromixing are compartmental models (Villermaux, 1991). In particular, Marini and Georgakis (1984a,b) and later Ochs et al. (1996) used a three-compartment model that was essentially one large CSTR and two small CSTRs with some recycle from the large CSTR to the small ones. This model is a compartment representation of the imperfect mixing of the inlet jet with the liquid bulk (Marini and Georgakis, 1984b). There was good agreement with LDPE experimental data (Marini and Georgakis, 1984b), and the effect that imperfect mixing had on polymer properties was studied (Marini and Georgakis, 1984a; Ochs et al., 1996).

Chan et al. (1993) used a CSTR followed by a plug-flow segment (represented by a number of CSTRs) to model each section of a multicompartment autoclave. There was recycle between each section of the model. The parameters to be fit in this model, therefore, were the recycle ratios and the number of CSTRs needed to model the plug-flow segment of each section. Fitting the preceding parameters along with some kinetic parameters, they showed that they could fit temperature, initiator flow, and conversion quite well as compared with a (multicompartment) industrial unit.

If we consider the autoclave reactor in the present work with reactor conditions shown in Table 3, correlations from the literature (Oldshue, 1983; Villermaux, 1991) provide a characteristic macromixing time for the reactor of approximately 22 s, while the residence time is about 30 s. Since the macromixing time is close to the residence time, there is a possibility of some adverse macromixing effects.

Micromixing in LDPE reactors

Much recent work on micromixing seems to have been done on the initial contacting of fluids, for instance, a feed stream entering a reactor (Villermaux, 1992). This is especially important for LDPE polymerization because cold monomer and initiator are fed into the hot reactor, forming a plume near the inlet, which is high in concentration of initiator.

Some phenomenological micromixing models have been used to study polymerization reactors:

- *Interaction by Exchange with a Mean Environment Model (IEM) (Villermaux et al., 1984).* In this model, the segregated region and the environment around this region exchange mass reversibly, with the driving force being the concentration difference between the segregated region and the average of the environment.
- *Erosion Model (Villermaux et al., 1984).* This model assumes that the segregated volume of the entering stream is shrinking with increasing time, and the eroded material is mixed with the bulk.
- *Plume Model (Zwietering, 1984).* This model assumes an exponential growth in the feed-stream plume. Eventually, the concentration inside the plume is the same as the bulk. The growth rate can be controlled with a micromixing parameter.
- *Engulfment Model (Smit, 1992).* Similar to the preceding, this model describes a growing reaction zone or plume as a function of the kinematic viscosity and the turbulent-energy dissipation rate.

Two other micromixing models that deserve mention, but were not specifically applied to LDPE reactor models include:

- *Layer Model (Zessin et al., 1992).* This model describes micromixing by diffusion in layers and is applied to fast reactions, for example, free-radical reactions.
- *Recirculation Model (Molen and Heerden, 1972).* This model is still a semiempirical model where micromixing is controlled by recirculation rate; it is able to describe experimental initiator productivity vs. temperature.

There is a least one parameter (or function) to fit in all of these schemes. All have succeeded in the sense that they can all describe, for instance, the experimentally observed minimum in the initiator consumption with increasing reactor temperature.

Partial segregation in LDPE reactors was studied via an erosion model and the IEM model by Villermaux (1984) for production of LDPE in a 0.9-L CSTR over 55 runs as a function of temperature, pressure, and choice of initiator. One interesting result was the calculation of minimum micromixing time. The micromixing time for the erosion model was found to be (Villermaux et al., 1984)

$$t_e = 8.9\times10^{-9}\exp\frac{-(-9{,}550+0.53P)}{T}, \qquad (1)$$

and for the IEM model, the relation was

$$t_m = 1.1\times10^{-9}\exp\frac{-(-10{,}100+0.57P)}{T} \qquad (2)$$

for P in bars, T in kelvins, and t in seconds. For the particular polymerization in this article at typical conditions, $T = 523$ K, $P = 2{,}020$ bar, the micromixing times are

$$t_e = 0.098 \text{ s} \qquad (3)$$

$$t_m = 0.030 \text{ s} \qquad (4)$$

With characteristic reaction time of around 1 s at 523 K (Figure 1), this result seems to indicate that micromixing has a very small effect on the polymerization; however, at 560 K

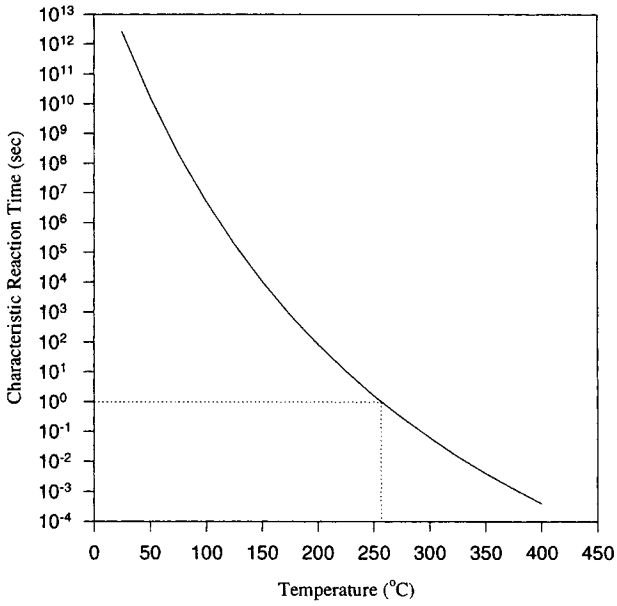

Figure 1. Charasteristic reaction times vs. reactor temperature.

Here $1/k_D$ is the characteristic reaction time for the decomposition of di-*tert*-butyl peroxide (DTBP). At typical reactor temperatures, the characteristic reaction time is around one second.

where the characteristic reaction time is on the order of 0.1 s or less, micromixing can be quite imperfect ($t_e = 0.03$, $t_m = 0.01$ at 560 K and 2,020 bar). If we assume that the 0.9-L reactor of Villermaux et al. (1984) behaves similarly to the 500-L reactor being studied here, then micromixing effects could be important in our case.

CFD simulation of a LDPE reactor

An approach to studying coupled mixing and reaction in the LDPE reactor that has received much attention recently (Torvik et al., 1995; Tsai and Fox, 1996) is computational fluid dynamics. Solving the flow field, species balances, and energy equation gives a view of all of the phenomena occurring in the reactor. Operating strategies can be tried off-line, resulting in safer and eventually more efficient production. Ranade summarized the recent advance in applying CFD simulation to reactor engineering (Ranade, 1995).

CFD simulation will give a solution for the macromixing in the reactor. Since the grid is much larger than the characteristic micromixing scale, CFD by itself will not include micromixing in its calculations. Micromixing then must be addressed in one of two ways: (1) empirical models relating the chemistry and the mixing; and (2) population balances on each cell. The advantages of the first method are ease of use, and small added computational burden; the disadvantage, though, is that parameters must be found for the empirical model. The population balance method overcomes this difficulty but imposes a large computational burden. Two articles are presented below that use CFD to simulate a LDPE reactor.

Torvik et al. (1995) simulated a 3-D multicompartment autoclave reactor using CFD, but without a micromixing model; this reactor had a stirrer that rotated at 200 rpm and had multiple injection points. Important results (Torvik et al., 1995) included:

- Verification of the k-ϵ turbulence model for a 1:1 scale autoclave was achieved.
- The temperature and concentration gradients were steepest close to the inlet.
- In their opinion, high-pressure autoclave reactors were overdesigned.

Another article (Tsai and Fox, 1996) simulated the front part of a tubular reactor. In this article, CFD was combined with a probability density function (PDF) method to simulate a 2-D axial section of the reactor. Because there were no impellers and because of either center or ring injection of the feed, there was an innate symmetry that justified the 2-D simulation. The main purpose of the PDF method was to determine in each cell the temperature and composition fields; therefore, a micromixing model was not needed. Assuming constant fluid properties, the authors implemented a two-step approach: (1) they first solved the flow using CFD; and then (2) they solved for the species and temperature fields with polymerization occurring. Although the subject in this article is the autoclave reactor, some of the conclusions (Tsai and Fox, 1996) are useful here. The conclusions were as follows:

- Mixing enhanced the initiator efficiency.
- Higher inlet temperature decreased initiator efficiency.
- Ring injection and increased mixing could be used to reduce hot spots.
- Most of the concentration and temperature gradients occurred near the inlet.

In the present work, a 3-D simulation of a LDPE autoclave is presented. Some interesting aspects of this work include: (1) this is a one-compartment autoclave; (2) use is made of an empirical micromixing reaction model outlined in "Simulation Strategy" section; (3) there is no symmetry, so a 3-D full-scale simulation is required; (4) mixtures of two initiators will be used in the feed; and (5) the k-ϵ turbulence model is used in the present work.

Theory

This section summarizes the theory of CFD simulation presented in this article. Basic governing equations, turbulence model, and turbulence-chemistry interaction are presented.

Governing equations

The governing equations for mass, momentum, heat, and species in a turbulent flow field with constant physical properties can be written as

$$\frac{\partial \rho}{\partial t} + \frac{\partial}{\partial x_i}(\rho u_i) = 0 \tag{5}$$

$$\frac{\partial}{\partial t}(u_i) + \frac{\partial}{\partial x_j}(u_i u_j) = -\frac{1}{\rho}\frac{\partial p}{\partial x_i} + \frac{1}{\rho}\frac{\tau_{ij}}{\partial x_j} + g_i \tag{6}$$

$$\frac{\partial h}{\partial t} + u_j \frac{\partial h}{\partial x_j} = \frac{k}{\rho C_p}\frac{\partial^2 h}{\partial x_j^2} - \tau_{ij}\frac{\partial u_i}{\partial x_j} + S_h \tag{7}$$

$$\frac{\partial C_\alpha}{\partial t} + u_j \frac{\partial C_\alpha}{\partial x_j} = D_{\alpha,m} \frac{\partial^2 C_\alpha}{\partial x_j^2} + S_\alpha(C), \tag{8}$$

where τ_{ij} is the viscous stress tensor defined by

$$\tau_{ij} = \mu\left(\frac{\partial u_i}{\partial x_j} + \frac{\partial u_j}{\partial x_i}\right) - \frac{2}{3}\mu \frac{\partial u_l}{\partial x_l}, \tag{9}$$

$S_\alpha(C)$ is the chemical reaction production term, and S_h is the heat source or sink that also depends on chemical reaction.

Reynold averaging for turbulent flow

Because LDPE autoclaves operate under vigorous mixing, the reactor medium is under turbulent flow conditions. It is then necessary to employ proper turbulent models to represent the effects of turbulent fluctuations of velocity and scalar variables on the basic conservation equations.

The conservation equations for turbulent flows can be obtained from the basic governing equations using Reynolds averaging. The Reynolds averaging procedure decomposes a conserved scalar value ϕ into a mean value $\bar{\phi}$ and a fluctuating part ϕ':

$$\phi = \bar{\phi} + \phi'. \tag{10}$$

Substituting Eq. 10 into the general conservation Eqs. 5 to 8 and taking the time average over a long period of time yields the momentum, heat, and species balance equations:

$$\frac{\partial \bar{u}_j}{\partial t} + \bar{u}_j \frac{\partial \bar{u}_i}{\partial x_j} = -\frac{1}{\rho}\frac{\partial \bar{p}}{\partial x_i} + \nu \frac{\partial^2 \bar{u}_i}{\partial x_j^2} - \frac{\partial}{\partial x_j}\overline{u_i' u_j'} + g_i \tag{11}$$

$$\frac{\partial \bar{h}}{\partial t} + \bar{u}_j \frac{\partial \bar{h}}{\partial x_j} = \frac{k}{\rho C_p}\frac{\partial^2 \bar{h}}{\partial x_j^2} - \frac{\partial}{\partial x_j}\overline{u_j' h'} + \overline{S_h(C)} \tag{12}$$

$$\frac{\partial \bar{C}_\alpha}{\partial t} + \bar{u}_j \frac{\partial \bar{C}_\alpha}{\partial x_j} = D_{\alpha,m}\frac{\partial^2 \bar{C}_\alpha}{\partial x_j^2} - \frac{\partial}{\partial x_j}\overline{u_j' C_\alpha'} + \overline{S_\alpha(C)}. \tag{13}$$

The resulting Reynolds averaged equations contain new unclosed correlations: Reynolds stresses, $\overline{u_i' u_j'}$, mass flux $\overline{u_i' C_\alpha'}$, enthalpy flux, $\overline{u_i' h'}$, mean reaction rate $\overline{S_\alpha(C)}$, and mean heat-source term $\overline{S_h(C)}$. These correlations can be closed by expressing them in terms of mean flow quantities, for example, using the k-ϵ model.

The k-ϵ turbulence model

The k-ϵ turbulence model is an eddy-viscosity model that relates Reynolds stress to the mean-velocity gradient through Boussinesq's hypothesis:

$$\rho\overline{u_i' u_j'} = \rho\frac{2}{3}k\delta_{ij} - \mu_t\left(\frac{\partial \bar{u}_i}{\partial x_j} + \frac{\partial \bar{u}_j}{\partial x_i}\right), \tag{14}$$

where $k = \frac{1}{2}\overline{u_l' u_l'}$ is the turbulent kinetic energy, μ_t is the turbulent eddy viscosity, and ϵ is the dissipation rate of k. μ_t is calculated based on the velocity scale ($\sqrt{k}$) and the length scale ($\sqrt{k^3}/\epsilon$):

$$\mu_t = \rho C_\mu \frac{k^2}{\epsilon}, \tag{15}$$

where C_μ is a constant. The transport equations for k and ϵ are given by

$$\frac{\partial k}{\partial t} + \frac{\partial \bar{u}_i k}{\partial x_i} = \frac{\partial}{\partial x_i}\left(\frac{\nu_t}{\sigma_k}\frac{\partial k}{\partial x_i}\right) + G_k - \epsilon \tag{16}$$

$$\frac{\partial \epsilon}{\partial t} + \frac{\partial \bar{u}_i \epsilon}{\partial x_i} = \frac{\partial}{\partial x_i}\left(\frac{\nu_t}{\sigma_\epsilon}\frac{\partial \epsilon}{\partial x_i}\right) + C_1\frac{\epsilon}{k}G_k - C_2\frac{\epsilon^2}{k} \tag{17}$$

where C_1 and C_2 are empirical constants, σ_k and σ_ϵ are Prandtl numbers for turbulent diffusion of k and ϵ, and G_k is generation rate of k:

$$G_k = \nu_t\left(\frac{\partial \bar{u}_i}{\partial x_j} + \frac{\partial \bar{u}_j}{\partial x_i}\right)\frac{\partial \bar{u}_i}{\partial x_j}. \tag{18}$$

The turbulent kinematic viscosity, ν_t, is related to k and ϵ through,

$$\nu_t = \frac{\mu_t}{\rho} = C_\mu \frac{k^2}{\epsilon}. \tag{19}$$

The following values of the parameters are used in the simulation:

$$C_1 = 1.44, \quad C_2 = 1.92, \quad C_\mu = 0.09, \quad \sigma_k = 1.0, \quad \sigma_\epsilon = 1.3. \tag{20}$$

Turbulence–reaction interaction

Modeling the source terms $\overline{S_\alpha(C)}$ and $\overline{S_h(C)}$ requires the description of turbulence–reaction interaction. The turbulent–reaction model of Magnussen and Hjertager (1976), which originates from the combustion area, is employed. Its main purpose is to limit the reaction rate when the reaction rate is faster than the rate of intermixing on the molecular scale. Using the empirical constants, k, the kinetic energy of the turbulent eddies, and ϵ, the rate of their dissipation, the following reaction rate arises:

$$R_{i',k} = C\rho\frac{\epsilon}{k}\frac{m_{i'}}{\nu_{i',k}'}, \tag{21}$$

where C is an empirical constant (4.0 for reactants and 2.0 for products), ρ is the density, $m_{i'}$ is the mass fraction of species i', and $\nu_{i',k}'$ is the stoichiometric coefficient of component i'. For each reaction k, Eq. 21 is computed for each species i'. The lowest reaction rate is chosen, and this is compared to the kinetic reaction rate. The lower of these two—the turbulent vs. the kinetic—reaction rates is taken to be the actual reaction rate.

Solution of equations

The conservation equations describing the fluid are solved through a control volume method (Fluent Inc., 1993). The geometric element, such as a reactor, is divided into a number of smaller elements called cells; this type of grid is termed the physical grid. The computational grids, on which the calculation is performed, are made up of regular cubes, and when it is deformed to fit the geometry of the problem, it becomes the physical grid.

The equations to be solved are in general partial differential equations. In each cell of the computational grid, these equations are solved by using the "Gauss Divergence Theorem," which changes volume integrals into surface integrals:

$$\int_A (v \cdot n)\, dA = \int_V (\text{div}\, v)\, dV, \tag{22}$$

where

$$v = Li + Mj + Nk \tag{23}$$

is a vector field defined on a domain of the space; i, j, k are unit vectors associated with x, y, z direction; and n is a normal vector to the surface. Also, defined in this domain is a closed region V and the piecewise smooth surface A that forms its boundary.

In each control volume, the differential equations are satisfied. Using Eq. 22, the quantity being solved is obtained on the surface of the cell. Special interpolation schemes are then used to determine the value of the quantity at the center of the computational cell (and *vice versa*), which is where the solution is stored. The key idea is that after applying the Divergence Theorem, the system of equations is discretized, and these discretized equations are very easy to solve over the computational domain.

Free-radical polymerization kinetics

Only three reactions are considered here—initiation, propagation, and termination by combination. This limited kinetic scheme, shown in Table 1, was chosen for the following reasons:

- These three reactions constitute the simplest reaction scheme for this polymerization and control the small molecule concentration gradients and temperature gradients.
- The goal here is to obtain the flow, species, and temperature fields and not to obtain polymer properties such as molecular-weight distribution.
- Excess initiator in the feed is a probable cause of the reactor runaway; this was verified via simulation. Macromixing has a significant effect on initiator decomposition.
- Propagation is significant and fast. This reaction accounts for the bulk of the energy released for this reactor system and is thus vital for the energy balance.
- The termination reaction is included so that the free-radical concentration in the reactor can be calculated. The quasi-steady-state assumption is not used. Termination is considered only by coupling (Chen et al., 1976).

Table 1. Polymerization Kinetics used in the CFD Model*

Name	Reaction	Rate
Initiation	$I \rightarrow 2R\cdot$	$2fk_d[I]$
Propagation	$M + R\cdot \rightarrow R\cdot$	$k_p[M][R\cdot]$
Termination	$R\cdot + R\cdot \rightarrow P$	$k_{tc}[R\cdot]^2$

*Note here that no distinction is made between the radical formed by the decomposition of the initiator and the live polymer.

Reactor Configuration and Simulation Strategy

Reactor configuration

The particular reactor configuration for the high-pressure autoclave was chosen based on information from the literature (Christl and Roedel, 1959; Gemassmer, 1977, 1978). A selection of this information is given in Table 2, and our choice for reactor variables is shown in Table 3. Two types of impeller design were implemented: four flat paddles and two flat paddles with two pitched-blades paddles.

Table 2. Some Suggested Design Parameters for Reactor*

Description	Variable	Recommendation	Source	Value Used
Length (height) of reactor to dia.	L/D	2.0–5.0	1	2.5
Volume	V	Varies (some > 1,000 L)	1,2	
	V	Up to 0.7 m^3	3	0.498 m^3
Dia. of inlet and outlet pipes	d_p	Very small (schematic)	1,2,4	0.02 m
Dia. of shaft	d_s	≈ 0.1 m from schematic (scaled)	1,2,4	0.08 m
Dia.: impeller vs. reactor	d_I/D	0.33–0.7 for turbines	5	
	d_I/D	0.6–0.7 schematic	1,2	0.6
	d_I/D	0.67 for paddles	6	
Impeller: hght. dia.	d_H/d_I	1/5 to 1/8 for turbines	5	0.2
	d_H/d_I	0.1 for paddles	6	
Impeller: depth (thickness) vs. diameter	d_w/d_I	1/20 for bar turbines	7	1/20
No. of impellers	n_{imp}	7 for $L/D = 2.5$ (schematic)	1,2	
	n_{imp}	5 for $L/D = 3.2$ (schematic)	4	
	n_{imp}	3 for $2.0 \le L/D \le 2.5$ (turbines)	7	4

*Sources: 1 (Gemassmer, 1977); 2 (Gemassmer, 1978); 3 (Doak, 1986); 4 (Christl and Roedel, 1959); 5 (Perry and Green, 1984); 6 (Engineering Equipment Users Association, 1963); 7 (McDonough, 1992).

Table 3. Design Variables for Reactors

Design Variable	Value
Vol. of reactor, V	0.498 m^3
Hght. of reactor, L	1.59 m
Dia. of reactor, D	0.64 m
Inlet and outlet pipe dia., d_p	0.02 m
Impeller dia., d_I	0.40 m
Impeller height, d_H	0.08 m
Impeller width (thickness), d_w	0.02 m
Dia. of shaft, d_s	0.08 m
No. of paddles, n_{imp}	4

Figure 2 shows the reactor configuration with pitched-blade impellers. The flat-paddle design is exactly the same except that all the impellers are flat paddles. The inlet is in the lower left corner at $x = 0$ (the axes are shown in the lower left corner of the figure). The reactor inlet is at the top of the reactor, that is, gravity points in the positive x-direction in Figure 2. They rotate at 250 rpm in the clockwise direction from an observer looking in the direction of the positive x-axis.

Simulation strategy

Full 3-D simulation has to be employed because symmetry is lost due to irregular impeller shape and out of center feed and outlet points. The reactor is first discretized into mesh cells, and conservation equations are solved for each cell. Figure 3 shows the surface grids around the impeller. Figure 4 shows a closer look around the impeller. A total of $54 \times 18 \times 46$ or 44,712 mesh cells are used to ensure good resolution.

There are a few assumptions and simulation strategies that must be addressed. Some of these assumptions are required by the structure of the CFD package; others save computation time.

First, it is assumed that the flow field is not influenced by concentration and temperature fields. Because monomer conversion is always low and natural convection effects are negligible, this assumption is thought to be reasonable. This assumption allows a two-step approach. First, the flow field is simulated at nominal conditions, and then the species and temperature fields are calculated. The reaction medium is assumed to be a Newtonian fluid because under the typical reaction conditions (200–300°C, 1,000–3,000 atm) the ethylene exists as a supercritical fluid and polymer content is low (10–15%).

The reactor is assumed to be adiabatic with cooling only by the fresh, cold feed. The heat capacity and thermal conduc-

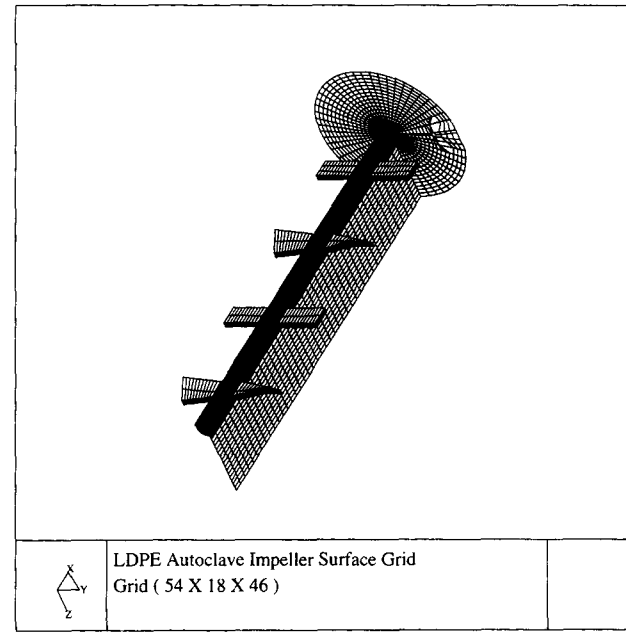

Figure 3. Surface grid around the impeller.

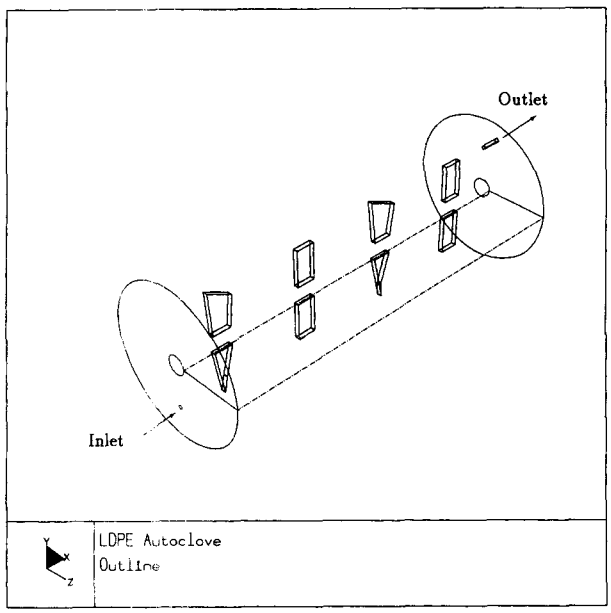

Figure 2. Reactor in fluent.
Showing the reactor setup with pitched-blade impeller.

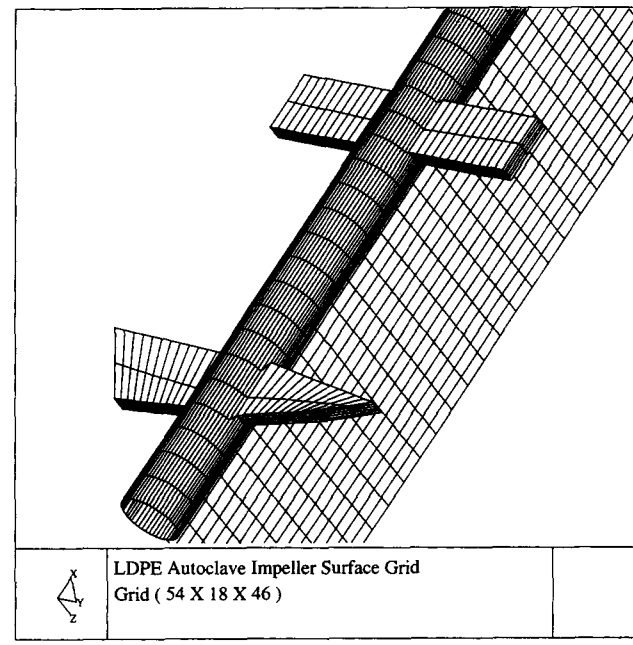

Figure 4. Surface grid around the impeller; close look.

Table 4. Physical Constants and Operating Parameters for Simulating the Nonisothermal Polymerization

Name	Value
Impeller speed, ω	250 rpm
Inlet velocity, v_{in}	53.3 m/s
Viscosity, μ	1.6×10^{-3} kg/ms
Density of mixture, ρ	499 kg/m^3
Inlet temperature, T_{in}	90°C
Activation energy for decomposition—DTBP, E_{aD}	1.612×10^{8} J/kmol
Preexponential factor for decomposition—DTBP, k_{oD}	9.05×10^{15} s^{-1}
Activation energy for decomposition—TBPOA, E_{aD}	1.494×10^{8} J/kmol
Preexponential factor for decomposition—TBPOA, k_{oD}	1.06×10^{16} s^{-1}
Initiator efficiency, f	1.0
Activation energy for propagation, E_{aP}	2.568×10^{7} J/kmol
Preexponential factor for propagation, k_{oP}	1.140×10^{7} m^3/kmol·s
Activation energy for termination, E_{aT}	1.268×10^{7} J/kmol
Preexponential factor for termination, k_{oT}	3.000×10^{9} m^3/kmol·s
Thermal conductivity of mixture, k	0.1998 J/m·s·K
Heat capacity of mixture, C_p	2768.0 J/kg·K
Decomposition heat of reaction—DTBP, TBPOA, $\Delta H_{rxn,D}$	2.092×10^{7} J/kmol
Propagation heat of reaction, $\Delta H_{rxn,P}$	-8.954×10^{7} J/kmol
Termination heat of reaction, $\Delta H_{rxn,T}$	-4.184×10^{6} J/kmol

tivity of the mixture in the reactor are assumed constant. All of the constants and operating parameters can be found in Table 4. The physical constants are selected assuming a reactor temperature of 250°C and a conversion of 15%. Around this temperature and conversion, the assumptions are considered to be reasonable.

To simplify boundary conditions, a rotating reference frame is used; the solution is from the viewpoint of an observer on the impeller. The flow field can be transformed back to a stationary coordinate system, but the concentration and temperature fields cannot. This should be apparent when the separate figures are presented.

Last, the computational burden is determined by two factors. The first is the number of state variables, that is, velocities, turbulence quantities, species concentrations, and enthalpy. As mentioned earlier, by solving the problem in a two-step manner this part of the computational burden can be alleviated. The second factor is the number of cells in which all of the equations must be solved. A total of 44,712 cells are used in the simulation; this number of cells is necessary to give good resolution to the simulation results. It takes approximately one week CPU time to get nonisothermal steady-state results on a HP-9000/715 workstation.

Results and Discussion

The simulation results are given in this section. The flow-field solutions are presented for both flat-paddle and the combination flat-/pitched-blade impeller designs. The reaction and turbulent mixing rates are compared for different reactions in order to determine whether the reactions are kinetic or mixing controlled. The results of the LDPE polymerization with different initiator combinations are given. Two initiators are used: DTBP (di-*tert*-butyl peroxide) and TBPOA (*tert*-butyl peroxyacetate). Table 5 gives the inlet initiator concentrations for each case.

Solution of the flow field

Due to very short residence time, good mixing is important for desired reactor operation. The flow fields of two different impeller designs are compared to decide which design gives better mixing patterns. At 250-rpm impeller speed, the flow field inside the reactor is highly turbulent. The k-ϵ turbulent model is employed to describe the turbulent flow field.

Figure 5 shows the axial velocity profile inside the reactor with flat-paddle impellers; Figure 6, the same profiles with two flat paddles replaced by pitched-blade paddles. In both cases, there is a large jet inlet effect due to fast inlet velocity (60 m/s). The pitched-blade impeller design gives much better turbulent mixing than the flat-paddle impellers.

Figures 7 and 8 compare the radical velocity profiles with the flat-paddle and pitched-blades impellers. Similar to the axial velocity profiles, pitched-blade impeller design gives more turbulent mixing as compared to flat-paddle impeller.

Based on the flow patterns, the combination of the flat- and pitched-blade paddles was chosen over flat-paddle design. The polymerization simulation results presented in the following section are based on the flat/pitched-blade impeller design.

Reaction and turbulent micromixing

In a turbulent reaction medium, two rate processes occur at the same time: reaction and turbulent mixing. Depending on the relative magnitude of reaction and turbulent mixing, the overall reaction rate is controlled by the slower rate-limiting steps. In free-radical polymerization of ethylene at high pressure, three main elementary reactions exist: initiation, propagation, and radical termination. These three reactions

Table 5. Initiator Feed Concentrations for all Cases*

Case	Initiator Composition	DTBP (ppm)	TBPOA (ppm)	Total (ppm)
I	100% DTBP	12	0	12
II	75/25 DTBP/TBPOA	9	3	12
III	50/50 DTBP/TBPOA	5	5	10
IV	25/75 DTBP/TBPOA	2.5	7.5	10

*All concentrations are on a mass basis.

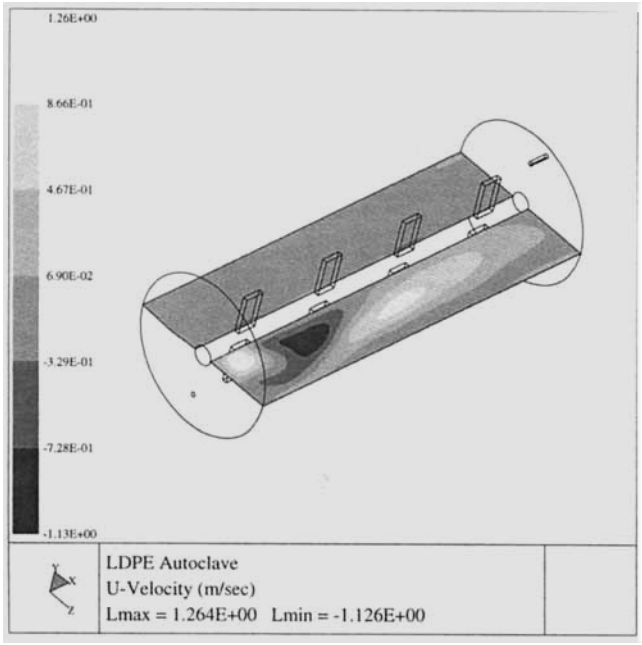

Figure 5. Axial velocity profiles with flat-paddle impellers.

The flat-paddle design does not provide adequate axial mixing.

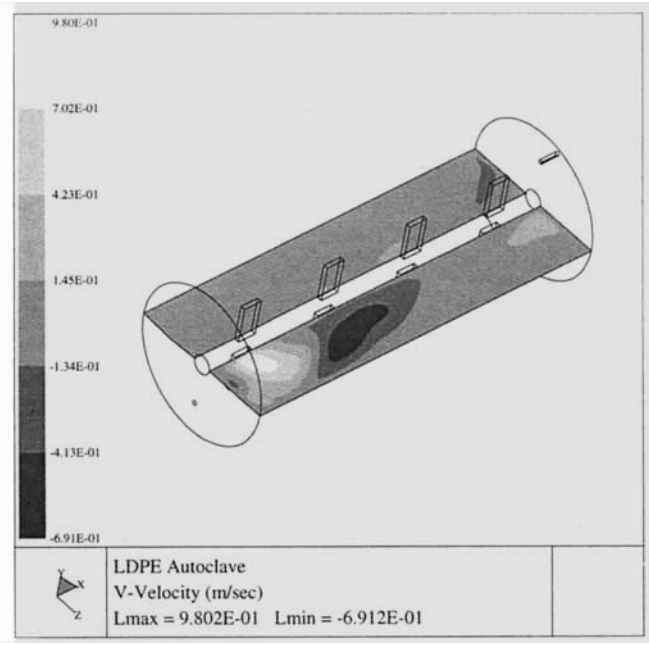

Figure 7. Radial velocity profiles with flat-paddle impellers.

The pitched-blade impellers give better radial mixing.

occur at different rates, and it is important to determine whether they are kinetic or mixing controlled.

Figure 9 compares the rates of turbulent mixing and initiator (DTBP) decomposition at different temperature, initiator concentration, and mixing intensity. Over the range of typical operation conditions, the turbulent micromixing rate is at least one order of magnitude higher than the initiation reaction rate. This suggests that under the conditions in this study, initiation reaction is the rate-limiting step; the turbulent mixing rate does not affect the initiation kinetics. However, at very high temperatures, above 580 K, the reaction rate increases rapidly with temperature due to high activation energy of initiation reaction (about 60 kcal/mol), whereas the

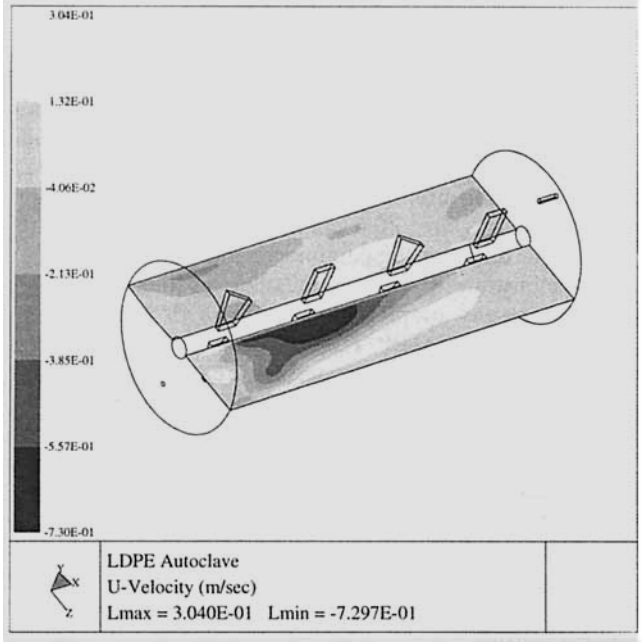

Figure 6. Axial velocity profiles with pitched-blade impellers.

The pitched-blade impellers give better axial mixing.

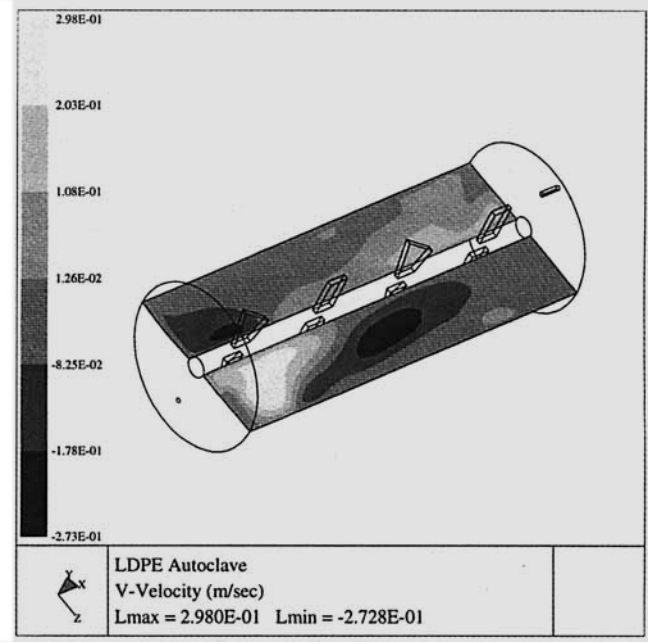

Figure 8. Radial velocity profiles with pitched-blade impellers.

The pitched-blade impellers give better radial mixing.

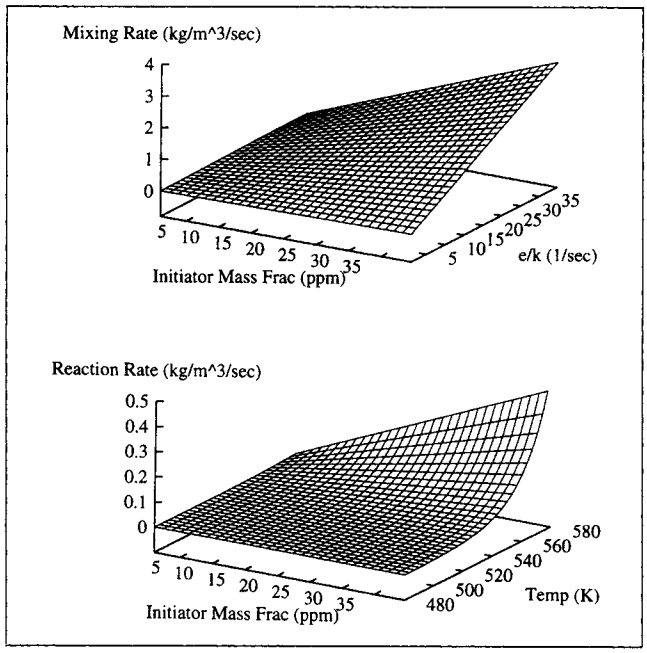

Figure 9. Initiator decomposition rate and micromixing rate.

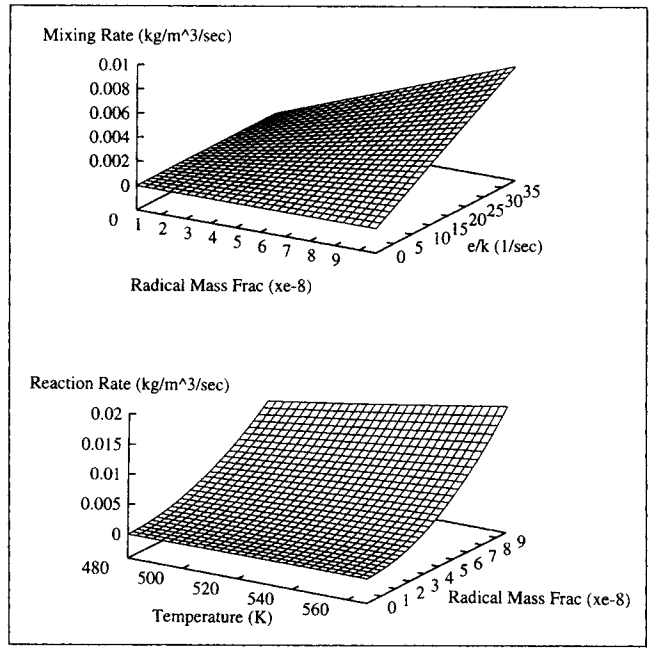

Figure 11. Termination rate and micromixing rate.

turbulent mixing rate is a weak function of temperature. The turbulent mixing can overcome reaction, and becomes the rate-limiting step at very high temperatures.

Figure 10 compares the propagation rate and corresponding turbulent mixing rate for typical operating parameters. Similar to initiation, the propagation rate is at least two orders of magnitude higher than the mixing rate, indicating that the reaction kinetics are the rate-limiting step under typical operating conditions.

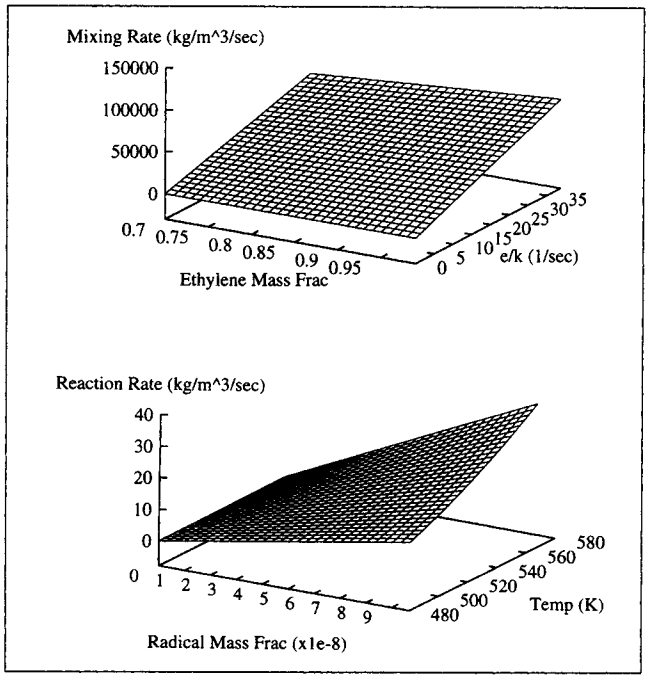

Figure 10. Propagation rate and micromixing rate.

However, the relative magnitudes of reaction and mixing are changed for free-radical termination reactions. Figure 11 compares the rates of turbulent mixing and termination of radicals by combination. Over the typical operation range, the mixing and reaction rates are in the same order of magnitude, with reaction rate larger in most of the cases. These results are expected because termination of two highly reactive radicals is an extremely fast reaction. This suggests that both reaction and turbulent mixing have to be considered in the simulation.

3-D simulation results

The polymerization was studied as four cases that are listed in Table 5. Each case uses a different proportion of two initiators, DTBP and TBPOA. DTBP is a high-temperature initiator and TBPOA is a low-temperature initiator. In industrial practice, mixture of initiators with different decomposing temperatures are often employed to maximize initiator efficiency at different temperature regions.

To demonstrate the CFD simulation capability, some 3-D simulation results are presented with case III (inlet initiator composition 50/50 DTBP/TBPOA) used as an example. For all the 3-D figures shown, the profiles are generated from the frame of reference of an observer on the impeller, or in the rotating reference frame.

Figure 12 shows the reactor temperature profile along the axial direction. Different from the typical assumption of uniform temperature in a CSTR, the temperature profile looks more like a plug-flow reactor with significant temperature gradient along the length of the reactor. This is caused by lack of a large axial circulation velocity (Figure 6) or inefficient backmixing.

Uniform temperature is more desirable due to uniform polymer structure and maximum reactor productivity. At low temperature the reaction rate is too slow; at high tempera-

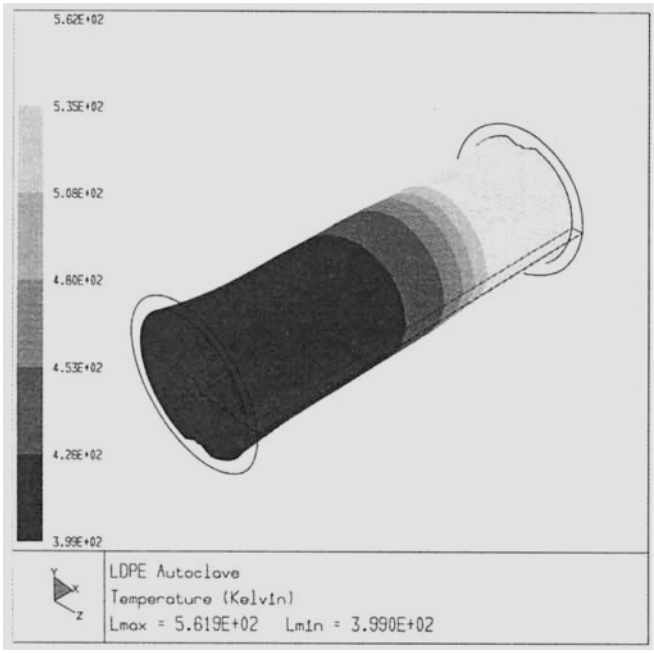

Figure 12. Case III: temperature profile.

The reactor temperature profile looks like plug flow and the outlet temperature approaches 290°C.

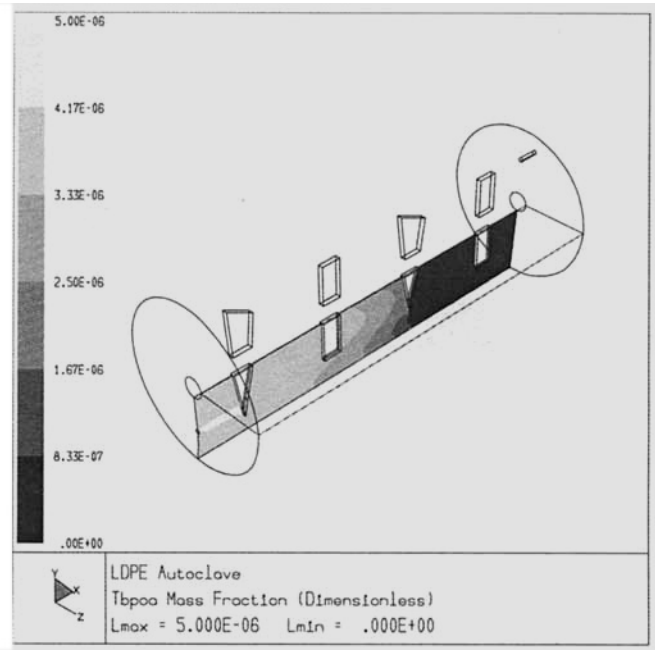

Figure 14. Case III: TBPOA concentration profile.

Feed plume exists near the feed point of the reactor due to fast decomposition rate of TBPOA.

ture the initiator decomposes too fast and it is very difficult to disperse the initiator well. From the CFD results, there is still some room to further improve the reactor operation by using multiple injection points, increasing impeller speed, and changing impeller design to improve axial mixing.

Figures 13 and 14 present the initiator (DTBP and TBPOA) concentration profiles along the axial direction of the reactor. For both initiators, initiators are burnt out at the bottom part of the reactor due to high temperature near the reactor outlet. Because of very low initiator concentration at the reactor bottom, that part of reactor volume is almost wasted. Methods to improve initiator consumption efficiency include multiple initiator injection to the bottom of reactor, lowering outlet temperature, and using an initiator with a higher decomposing temperature.

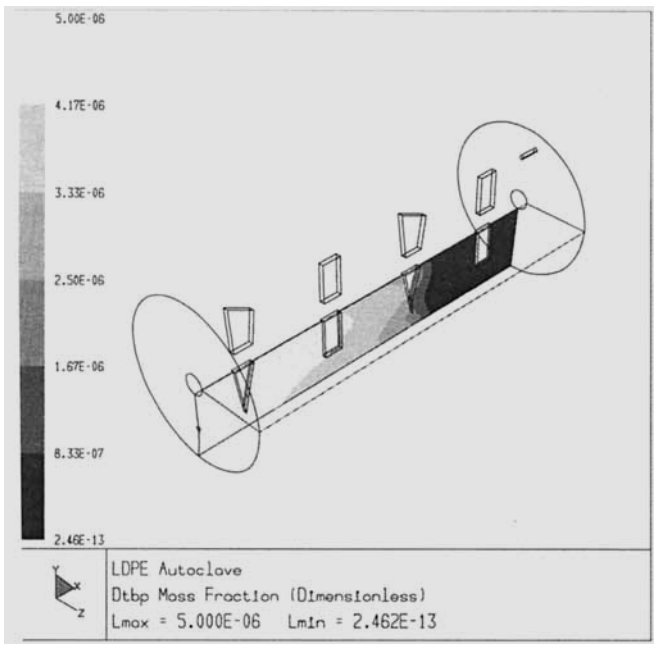

Figure 13. Case III: DTBP concentration profile.

Due to high temperature at the reactor bottom, DTBP almost burns out at the reactor bottom.

Some distinct differences exist between DTBP and TBPOA concentration profiles at the top part of the reactor. Since TBPOA is a low-temperature initiator, it decomposes very fast even at the low temperature. A high-concentration plume can be clearly seen near the reactor inlet. At a very fast decomposition rate, it is difficult to mix the initiator feed well. However, for the high-temperature initiator DTBP, there is no high-concentration plume; the initiator concentration is also more uniform in the top part of the reactor.

The initiator is fed directly toward the tip of the first impeller blade at high velocity. Dispersion of the initiator by the rotation of the impeller causes a lot of the initiator to be concentrated in this region. It also cools this region because of the lower temperature of the feed. This configuration might be suboptimal. There have been suggestions (Christl and Roedel, 1959; Gemassmer, 1978) of using other feed designs so as to increase the mixing of reactants.

Figure 15 shows the free-radical concentration profile along the axial direction. Similar to other species, the radical concentration is not uniform; instead, the radical has maximum concentration at a certain length along the axial direction. The radical concentration is very low at both the top and the bottom part of the reactor due to low temperature at the top and high temperature burnout in the bottom. The maximum can be explained on the basis that reactor temperature increases from the top to the bottom, whereas the initiator con-

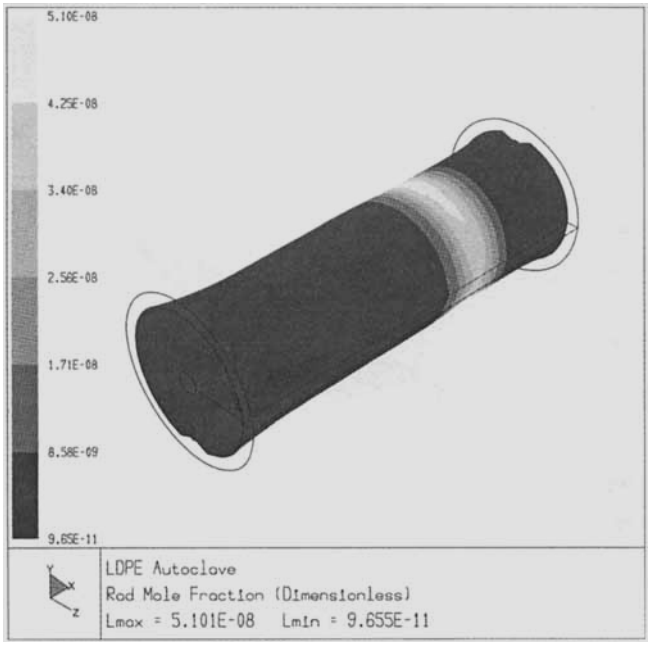

Figure 15. Case III: free-radical concentration profile.

Maximum radical concentration occurs at certain reactor length.

centration decreases from the top to the bottom. The combined effects of these two competing factors result in maximum radical concentration at a certain reactor length.

Figure 16 shows the polymer concentration profile along the axial direction; the profile is similar to the temperature profile. The conversion at the outlet is around 17%, which is typical for this type of autoclave reactor.

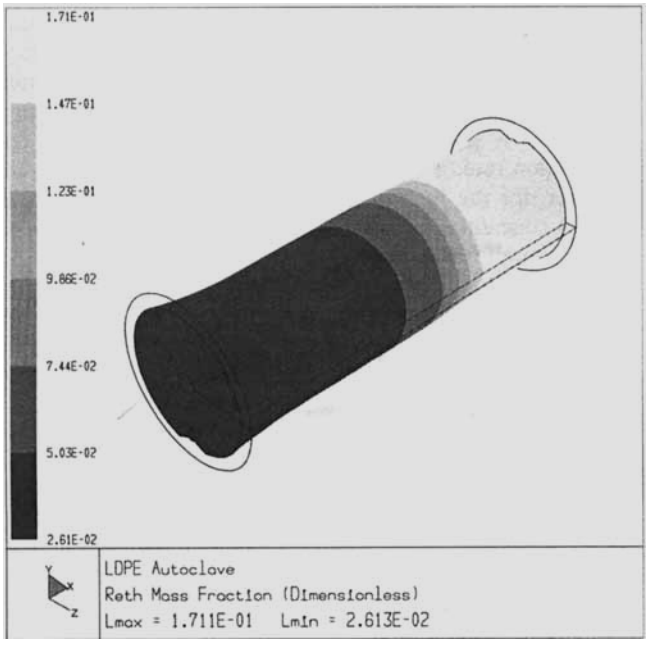

Figure 16. Case III: reacted-ethylene concentration profile.

The profile is similar to the temperature profile and looks like a plug-flow reactor.

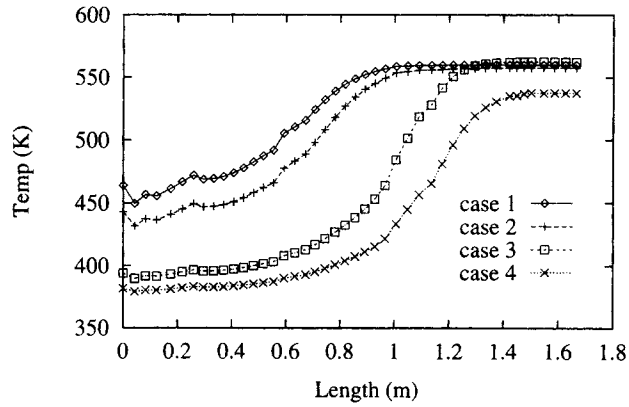

Figure 17. Reactor temperature along the jet line.

The jet line is parallel to the reactor axis.

Effects of inlet initiator composition

Due to the adiabatic nature of the LDPE autoclave, inlet initiator is the main operation variable used to control the reactor temperature. In this section, four different initiator compositions are studied. Instead of using the 3-D contour plots, 2-D profiles along the center of inlet line parallel to the reactor axial are used; they are more useful for quantitative comparison.

Figure 17 shows the temperature profile along the center of the feed line for four different inlet initiator compositions. Increasing TBPOA composition (from case I to case IV) decreases the reactor temperature at the same distance from the inlet point. The temperature difference between the reactor inlet and outlet also increases with increasing TBPOA composition.

The differences among the four cases are mainly due to differing decomposition rates of the two initiators. At each temperature in the range used here, the initiator TBPOA has roughly five times the decomposition rate of DTBP. This implies that to achieve polymerization conditions with the slower initiator, DTBP, a higher steady-state temperature must be achieved. As the amount of the slower initiator fed decreases, the temperature decreases also.

Figures 18 and 19 shows the concentration profiles of the two initiators, DTBP and TBPOA. With increasing TBPOA composition (from case I to case IV), DTBP concentration

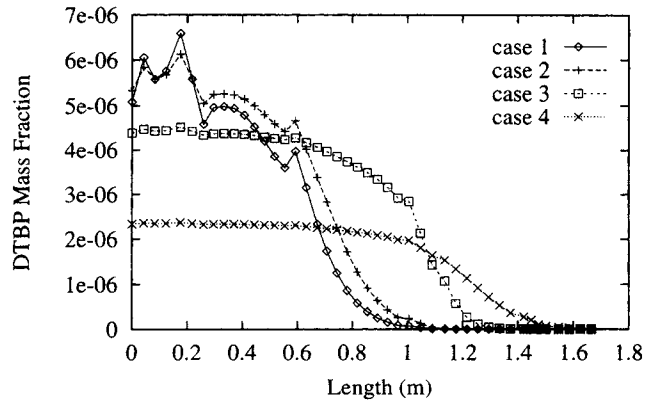

Figure 18. DTBP concentration along the jet line.

The jet line is parallel to the reactor axis.

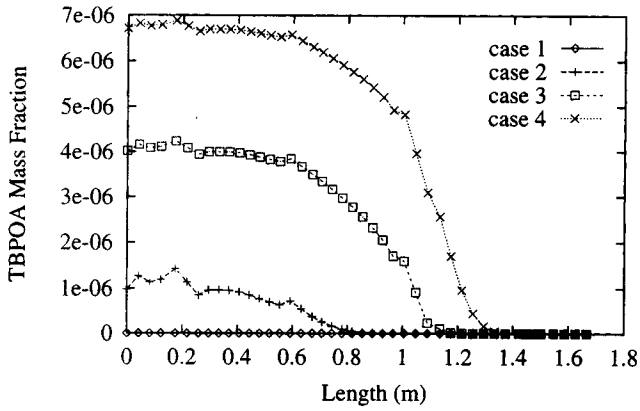

Figure 19. TBPOA concentration along the jet line.
The jet line is parallel to the reactor axis.

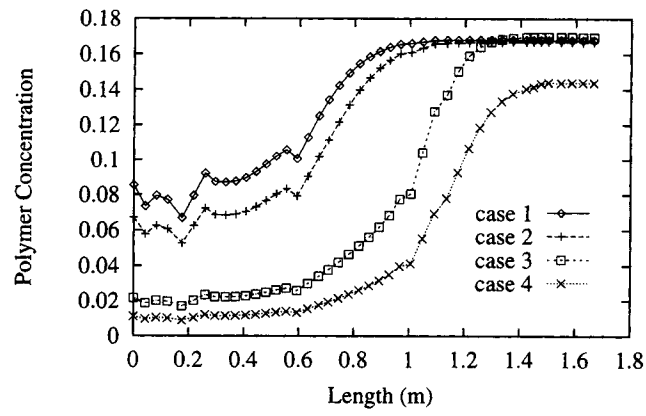

Figure 21. Polymer concentration along the jet line.
The jet line is parallel to the reactor axis.

profiles become less steep and initiator burnout occurs toward the end of reactor. The behavior of the TBPOA profiles is similar to DTBP, except that the concentration gradient and initiator burnout occurs at a closer distance to the inlet. These results are mainly caused by the lower decomposing temperature of TBPOA and the resulting lower temperature profile inside the reactor as shown in Figure 17.

The radical concentration profile along the jet line is presented in Figure 20. The radical concentration clearly shows a maximum along the reactor length. With increasing TBPOA concentration, the position of maximum radical concentration moves down the reactor length.

As explained before, the rate of radical formation is strongly influenced by the concentration of initiator and temperature. As the temperature increases, $[R\cdot]$ increases; as initiator concentration decreases, $[R\cdot]$ decreases. These two state variables interact in such a way as to create a maximum in the radical concentration.

Since temperature and initiator concentration profiles vary according to the composition and amount of initiator fed into the reactor, the maximum in the radical concentration also moves. As less of the slow initiator is added, and thus as the temperature in the front part of the reactor decreases, the maximum in radical concentration moves down the reactor.

Figure 21 presents the polymer concentration profile along the jet line. Increasing TBPOA composition, the monomer

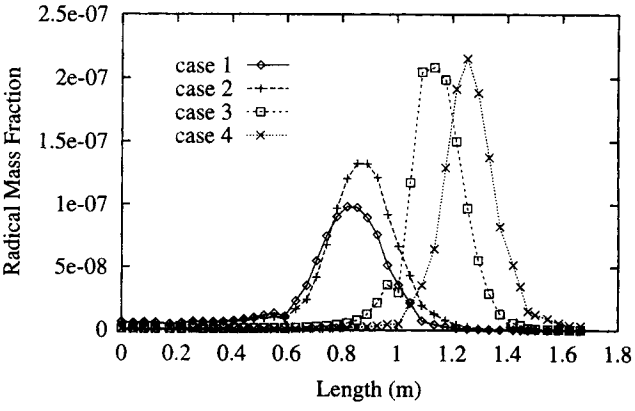

Figure 20. Free-radical concentration along the jet line.
The jet line is parallel to the reactor axis.

conversion near the outlet remains about the same to a certain point (cases I to III), then it decreases (case IV). The slower decomposing initiator results in an increase in temperature in the first part of the reactor; this causes the propagation rate to increase, which raises conversion. As the amount of the slower initiator, DTBP, fed into the reactor decreases, the conversion in the front part of the reactor decreases. While free radicals are produced by the faster initiator, the temperature is too low to favor the propagation reaction.

In general, it might be expected that as less of the slow initiator is added and thus the operating temperature is decreased, there would be less conversion. This is observed in the case studies. However, the situation can be even more complex. In cases III and IV, only 10 ppm of initiator is fed, as compared with 12 ppm for cases I and II. Nevertheless, case III has an outlet conversion of 17%, which is comparable to cases I and II. This happens because the end of the reactor is not wasted as it is in cases I and II. That is, initiator burnout occurs farther down the reactor in case III, resulting in more propagation toward the end of the reactor.

In case IV, initiator burnout also occurs near the outlet, but in this case because of the preponderance of fast initiator, the operating temperature does not reach the level that it does in case III, resulting in less propagation and thus less conversion. In simple terms, one sees that high operating temperature in the reactor increases conversion, and slow initiators lead to these high operating temperatures. High operating temperatures also cause initiator burnout and result in part of the reactor being wasted. Finally, high temperature brings the possibility of danger from the decomposition of ethylene, which occurs close to 300°C (Bonsel and Luft, 1995). All of these factors must be taken into consideration.

There appear to be two ways to improve the efficiency of the initiator while avoiding early burnout: (1) use of a combination of fast and slow initiators (as studied here) in a single compartment autoclave; or (2) use of a multicompartment autoclave with fresh initiator and monomer in each section. Both of these approaches are used industrially. As shown here, more efficient use of initiator can lead to improved reactor performance.

Conclusions

The steady-state operation of an industrial-sized LDPE reactor has been simulated using computational fluid dynamics.

This approach has allowed a distributed view of the reactor showing what kind of mixing occurs and what kind of composition and temperature fields exist. The results show that this reactor is definitely not a CSTR as commonly assumed in the literature.

As shown by the simulations, characteristics of this reactor system include a steep concentration of the initiator profile close to the inlet, a temperature that increases going down the reactor, a maximum in the radical concentration, a conversion that increases down the reactor, and great sensitivity to the amount and composition of initiator. All of these characteristics can be modified somewhat using a different reactor design and operation.

With a 50/50 mix of 10 ppm total DTBP and TBPOA initiators, case III seems to give the best results of the four simulations as far as initiator consumption and conversion are concerned. However, these simulations do not take into account the molecular weight or the molecular-weight distribution of the polymer produced.

The simulation results presented in this article are steady-state results with only polymerization kinetics included. Work is currently underway to include decomposition kinetics for runaway simulation and polymer molecular-weight moments; simulation of copolymerization systems are also planned. The results are to be presented in the upcoming articles.

Acknowledgments

We thank the industrial sponsors of the UW Polymerization Reaction Engineering Laboratory (UWPREL) for financial support. The authors are also indebted to Dr. Robin Hutchinson and Alex Schaffer of DuPont and Masashi Hamba of Sumitomo Chemical for helpful comments, and to Dr. Zhengfang Xu for suggestions during the revision. Last, we are grateful to Paul Oliphant at the Computer Aided Engineering Center (CAE) at UW-Madison for obtaining the relevant software and supplying a large amount of computation time.

Notation

c_p = mixture-specific heat, $J \cdot kg^{-1} \cdot K^{-1}$
D = reactor diameter, atm
$D_{\alpha,m}$ = diffusivity coefficient
d_H = impeller height, m
d_I = impeller diameter, m
d_p = inlet and outlet diameter, m
d_s = shaft diameter, m
d_w = impeller width, m
E_a = activation energy of Arrhenius equation, J/kmol
f = initiator decomposition efficiency
g_i = gravity force
$[I]$ = initiator concentration, $kmol/m^3$
k_{d_i} = initiator i decomposition rate constant, s^{-1}
k_o = pre-exponential factor of Arrhenius equation, $m^3 \cdot kmol^{-1} \cdot s^{-1}$
k_p = propagation rate constant, $m^3 \cdot kmol^{-1} \cdot s^{-1}$
k_{tc} = termination rate constant, $m^3 \cdot kmol^{-1} \cdot s^{-1}$
L = reactor height, atm
$[M]$ = monomer concentration, $kmol/m^3$
Mw = monomer molecular weight, k/mol
n_{impp} = number of impeller on the shaft
$[P]$ = polymer concentration, $kmol/m^3$
P = reactor pressure, atm
T_{in} = inlet feed temperature, °C
V = reactor volume, m^3
v_{in} = inlet feed velocity, m/s
x_j = spacial coordinate j
$\Delta H_{rxn,D}$ = heat of reaction of decomposition of initiator, J/kmol
$\Delta H_{rxn,P}$ = heat of reaction of propagation, J/kmol
$\Delta H_{rxn,T}$ = heat of reaction of termination, J/kmol
μ = viscosity, kg/m^3
ω = impeller speed, rpm
ρ_j = density of species j, kg/m^3

Literature Cited

Bonsel, H., and G. Luft, "Safety Studies on the Explosive Degradation of Compressed Ethene," *Chem. Ing. Tech.*, **67**, 862 (1995).
Chan, W.-M., P. E. Gloor, and A. E. Hamielec, "A Kinetic Model for Olefin Polymerization in High-Pressure Autoclave Reactors," *AIChE J.*, **39**, 111 (1993).
Chen, C. H., J. G. Vermeychuk, J. A. Howell, and P. Ehrlich, "Computer Model for Tubular High-Pressure Polyethylene Reactors," *AIChE J.*, **22**, 463 (1976).
Christl, R. J., and M. J. Roedel, "Constant Environment Process for Polymerizing Ethylene," U.S. Patent No. 2,897,183, duPont (1959).
Doak, K. W., "Low Density Polyethylene (High Pressure)," *Encyclopedia of Polymer Science and Engineering*, 2nd ed., Vol. 6, H. F. Mark, N. M. Bikales, C. G. Overberger, G. Menges, and J. I. Kroschwitz, eds., Wiley, New York, p. 386 (1986).
Engineering Equipment Users Association, *Agitator Selection and Design*, Constable & Co., London (1963).
Fluent Inc., *Fluent User's Guide, Version 4.2* (1993).
Gardner, G. M., *A Theoretical Study of the Kinetics of Polyethylene Reactor Decompositions*, Master's Thesis, Texas Tech Univ., Lubbock (1975).
Gemassmer, A. M., "The Autoclave Process for the High-Pressure Polymerization of Ethylene," *High Temp.—High Pressures*, **9**, 507 (1977).
Gemassmer, A. M., "Autoclave Process for the High Pressure Polymerization of Ethylene," *Erdol Kohle-Erdgas-Petrochem.*, **31**, 221 (1978).
Huffman, W. J., D. C. Bonner, and G. M. Gardner, "Decompositions in Polyethylene Reactors: A Theoretical Study," AIChE Meeting (1974).
Magnussen, B. F., and B. H. Hjertager, "On Mathematical Modeling of Turbulent Combustion with Special Emphasis on Soot Formation and Combustion," *16th Symp. (Int.) on Combustion*, Trondheim, Norway, p. 719 (1976).
Marini, L., and C. Georgakis, "The Effect of Imperfect Mixing on Polymer Quality in Low Density Polyethylene Vessel Reactors," *Chem. Eng. Commun.*, **30**, 361 (1984a).
Marini, L., and C. Georgakis, "Low-density Polyethylene Vessel Reactors Part I: Steady State and Dynamic Modelling," *AIChE J.*, **30**, 401 (1984b).
McDonough, R. J., *Mixing for the Process Industries*, Van Nostrand Reinhold, New York (1992).
Molen, J. V. D., and C. V. Heerden, "The Effect of Imperfect Mixing on the Initiator Productivity in the High Pressure Radical Polymerization of Ethylene," *Proc. of the 1st Int. Symp. on Chemical Reaction Engineering*, R. F. Gould, ed., Amer. Chem. Soc., p. 92 (1972).
Ochs, S., P. Rosendorf, I. Hyanek, X. Zhang, and W. H. Ray, "Dynamic Flowsheet Modelling of Polymerization Processes Using POLYRED," *Comput. Chem. Eng.*, **20**, 657 (1996).
Oldshue, J. Y., *Fluid Mixing Technology*, McGraw-Hill, New York (1983).
Perry, R. H., and D. Green, eds., *Perry's Chemical Engineers' Handbook*, 6th ed., McGraw-Hill, New York, p. 19-5 (1984).
Ranade, V. V., "Computational Fluid Dynamics for Reactor Engineering," *Rev. Chem. Eng.*, **11**, 229 (1995).
Smit, L., "The Use of Micromixing Calculations in LDPE-Reactormodelling," *4th Int. Workshop on Polymer Reaction Engineering*, K. H. Reichert and H. U. Moritz, eds., DECHEMA, p. 77 (1992).
Sullivan, J. F., and D. I. Shannon, "Decomposition Venting in a Polyethylene Product Separator," *Codes and Standards and Applications for High Pressure Equipment*, J. E. Staffiera, ed., ASME, New York, p. 191 (1992).

Torvik, R., A. R. Gravdahl, G. R. Fredriksen, O. Meon, and J. Laurell, "Design of HPPE Stirred Autoclaves using 3D Computational Fluid Dynamics," *Int. Workshop on Polymer Reaction Engineering*, K. H. Reichert and H. U. Moritz, eds., DECHEMA, Frankfurt, p. 401 (1995).

Tsai, K., and R. O. Fox, "PDF Modeling of Turbulent-Mixing Effects on Initiator Efficiency in a Tubular LDPE Reactor," *AIChE J.* **42**, 2926 (1996).

Villermaux, J., "Mixing Effects on Complex Chemical Reactions in a Stirred Reactor," *Rev. Chem. Eng.*, **7**, 51 (1991).

Villermaux, J., "Mixing in Polymer Reactors," *4th Int. Workshop on Polymer Reaction Engineering*, K. H. Reichert and H. U. Moritz, eds., DECHEMA, Frankfurt, p. 3 (1992).

Villermaux, J., M. Pons, and L. Blavier, "Comparison of Partial Segregation Models for the Determination of Kinetic Constants in a High Pressure Polyethylene Reactor," *ISCRE 8, Int. Symp. on Chemical Reaction Engineering*, Institution of Chemical Engineers, *Symp. Ser.*, **87**, p. 553 (1984).

Zhang, S. X., N. K. Read, and W. H. Ray, "Runaway Phenomena in Low-Density Polyethylene Autoclave Reactors," *AIChE J.*, **42**, 2911 (1996).

Zessin, J., U. Engelmann, G. Schmidt-Naake, H. J. Oelmann, and W. Pippel, "Influence of Micromixing on Free Radical Polymerization," *Int. Workshop on Polymer Reaction Engineering*, K. H. Reichert and H. U. Moritz, eds., DECHEMA, p. 67 (1992).

Zwietering, T. N., "A Backmixing Model Describing Micromixing in Single-Phase Continuous-Flow Systems," *Chem. Eng. Sci.*, **39**, 1765 (1984).

Manuscript received Dec. 4, 1995, and revision received July 1, 1996.